Observations of the ultraviolet and x-ray brightness profiles and cooling rates of Kr and Ar in magnetically confined fusion plasmas

M. J. May,[1] K. B. Fournier,[2] D. Pacella,[3] H. Kroegler,[3] J. E. Rice,[4] B. Gregory,[5] M. Finkenthal,[1,6] H. W. Moos,[1] G. Mazzitelli,[3] and W. H. Goldstein,[2]

[1]*Plasma Spectroscopy Group, Department of Physics and Astronomy, The Johns Hopkins University, 34th and North Charles Streets, Baltimore, Maryland 21218*

[2]*Lawrence Livermore National Laboratories, Livermore, P.O. Box 808 L41, Livermore, California 94551*

[3]*FTU, Associazione EURATOM ENEA sulla Fusione, Frascati (Roma), Italy*

[4]*Plasma Science and Fusion Center, Massachusetts Institute of Technology, 190 Albany Street, Cambridge, Massachusetts 02139*

[5]*Institut National de la Recherche Scientifique and Centre Canadien de Fusion Magnetique, Varennes, Canada*

[6]*Racah Institute of Physics, Hebrew University, Jerusalem, Israel*

(Received 1 July 1999; revised manuscript received 15 September 1999)

The spatial brightness profiles of Ar and Kr ions have been measured during a set of experiments in which these gases were puffed into FTU (Frascati Tokamak Upgrade) and Alcator C-Mod tokamak plasmas. These profiles were measured by spatially scanning photometrically calibrated vuv and x-ray spectrometers covering 3 to 1700 Å on a shot to shot basis. Several simulations of these profiles were performed using the multiple ionization state transport (MIST) code to validate the atomic physics rates used to determine the charge state distribution in the plasmas. A comparison of two sets of atomic physics rates was made. The chosen rates were the original rates in MIST and the more accurate ionization/recombination rate coefficients from the HULLAC atomic code and the current compilations by Mazzotta. The simulations with the more accurate rates could correctly predict the brightness profiles. The simulations with the older rates adequately predicted the Ar brightness profiles but did not accurately predict those of Kr. The inclusion of the excitation autoionization rates which were absent from the MIST code had the most profound effect on the simulated charge state distributions.

PACS number(s): 52.55.Fa, 52.25.Jm, 52.25.Fi, 52.65.−y

I. INTRODUCTION

Future magnetically confined fusion (MCF) devices will have severe heat loads and particle fluxes on both the armor tiles surrounding the core of the tokamak plasma and on the strike plates in the divertor region. Particles escape the plasma since they are trapped only for the plasma particle confinement time, or they are channeled along the last closed flux surface onto the divertor strike plates. Also, the heat from the fusion plasma is conducted and convected through the entire scrape-off layer to the strike plates. To withstand this harsh environment, the plasma facing tiles will need to be composed of high-Z refractory materials such as Mo ($Z=42$) and/or W ($Z=74$). In the MCF device the high-Z tiles have a predicted lifetime 300 times longer [1] than those made of carbon or beryllium. Unfortunately, even tiles composed of either Mo or W can be sputtered to an unacceptable degree, and their lifetime could be too short for their effective use in a reactor. Also, significant levels $[n_z(0)/n_e(0) \sim 10^{-4}]$ of these sputtered high-Z impurities could present a radiation problem since these elements are not fully stripped even at 10 keV [2,3]. This radiation could have deleterious effects on the fusion plasma by lowering the core temperature and degrading the energy confinement.

To reduce the localized heat flux onto the divertor plates and to distribute it evenly, a radiating mantle can be created near the last closed flux surface and/or in the divertor region. The edge plasma in this ''radiative divertor''scenario will be cooled by puffing a controlled amount of gas into either the plasma edge or the divertor. The plasma particles will collide with the puffed gas particles in this cooler region and lose a significant fraction of their kinetic energy. Therefore, the tile sputtering by the particles is reduced since the sputtering yield significantly decreases with decreasing particle energy [4]. The energy is radiated into 4π steradians instead of being directed to the plates. The coolant gases He, Ne, Ar, and Kr, have been puffed into DIII-D tokamak plasmas in San Diego for radiative divertor studies [5]. Ar, Kr, Ne, and N_2 have been puffed into the Alcator C-Mod tokamak plasmas with L and H-mode confinement [6] to produce ''detached'' divertors. Neon puffs were introduced into TEXTOR plasmas to determine the compatibility of high-Z armor tiles and a plasma having radiative improved-mode (RI-mode) confinement [7] with high ICRF power. JET has also experimented with detached divertor operation [8].

The spatial locations of the radiation for each coolant gas must be determined in order for them to be used effectively as a coolant. To determine the regions of cooling, the charge state distribution (CSD) and the cooling rate curve must be known. The CSD can be predicted using a plasma transport code with correct atomic physics rates and known anomalous plasma transport coefficients. The cooling rate curve can be calculated using an atomic physics package such as the Hebrew University Lawrence Livermore Atomic Code (HULLAC) [9,10,11]. To test the ionization/recombination atomic physics rates used in the CSD calculations for a coronal plasma (no transport), the spatial brightness profiles of two coolant gases, Ar and Kr, have been measured in FTU and Alcator C-Mod tokamak plasmas and simulated with the

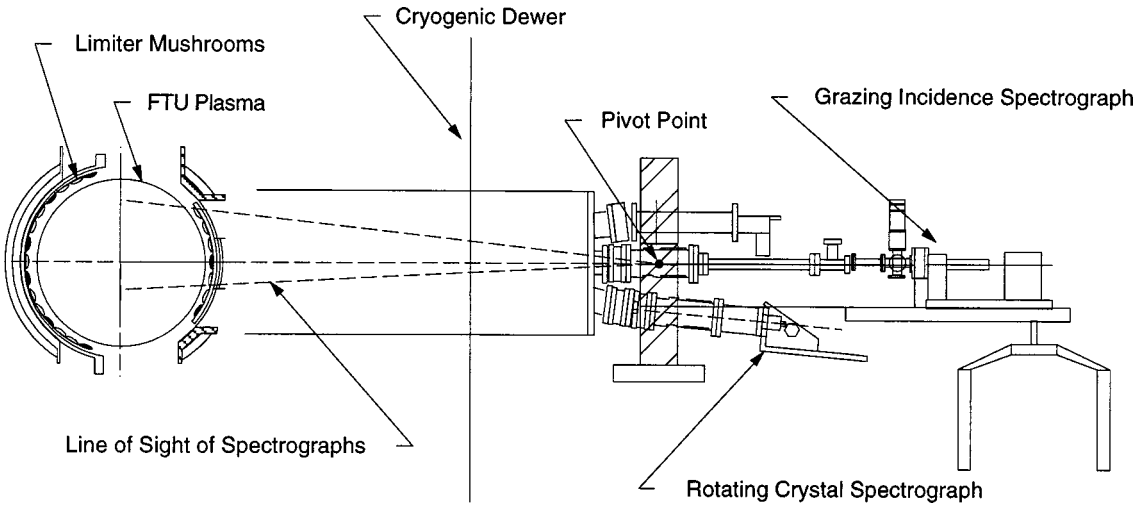

FIG. 1. Side profile of FTU tokamak.

multiple ionization state transport (MIST) code [12]. The ionization/recombination physics rates that were present in the MIST code were found to simulate the profiles reasonably well for Ar; the rates for Kr were found to be inadequate for the simulations. Agreement between the measured and simulated charge state distribution for Kr and better agreement for Ar was only possible with ionization/recombination rates computed from HULLAC and the rates from Mazzotta. These rates were calculated by using HULLAC and taken from the compilation of Mazzotta [13]. The inclusion of the excitation-autoionization (EA) processes had the most significant effect on the CSD since this ionization channel was absent in the original MIST atomic rates. The dielectronic recombination rate from HULLAC and Mazzotta differ from what was in MIST on average by ~50%. The new rates significantly shifted the CSD. A similar conclusion was reached by Rice *et al.* in their paper on molybdenum impurities observed in the Alcator C-Mod tokamak plasmas [14]. Two cooling curves are also compared in this work. The first was generated from ADPAK by Post [15]. The second was calculated from the HULLAC atomic data package and the new CSD. The HULLAC cooling curves could correctly predict the radiation from the plasma. The ADPAK cooling curves for Ar and Kr did not satisfactorily simulate the emissivities from the bolometery.

II. EXPERIMENT

A. FTU

During these experiments the FTU Tokamak (Fig. 1) operated with a plasma current, I_p, of 0.5 MA, a toroidal magnetic field, B_T, of 5.9 T, and an Ohmic input power, P_{Oh}, of $\sim$ 1 MW. The plasma was circular with a major radius of 96 cm and a minor radius of 30 cm with a working gas of hydrogen. FTU has no divertor configuration. The argon gas puffing experiments had a central electron temperature, T_{e0}, of 2.9 keV, and central electron density, n_{e0}, of 6.8 $\times 10^{13}$ particles/cm^3. The krypton gas puffing experiments had a T_{e0} of 1.7 keV and an n_{e0} of 7.7×10^{13} particles/cm^3. The density and temperature profiles are shown in Fig. 2. The lower electron temperature during the Kr experiments resulted from the higher cooling properties of Kr. The electron temperature was measured with Thomson scattering, and the electron density was determined with the far infrared radiation (FIR) laser or the ''DCN'' interferometer [16].

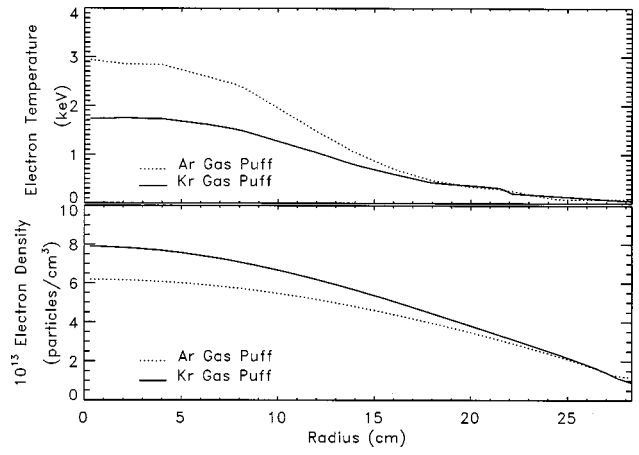

FIG. 2. Temperature and density profiles in FTU tokamak plasmas.

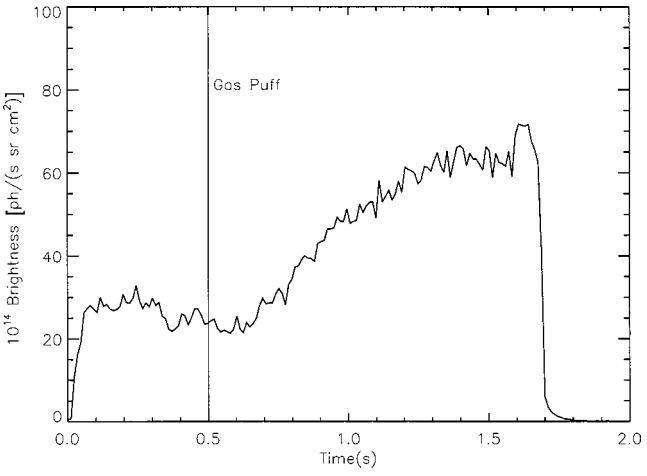

FIG. 3. Time history of Ar^{14+} line at 221.15 Å during a gas puff.

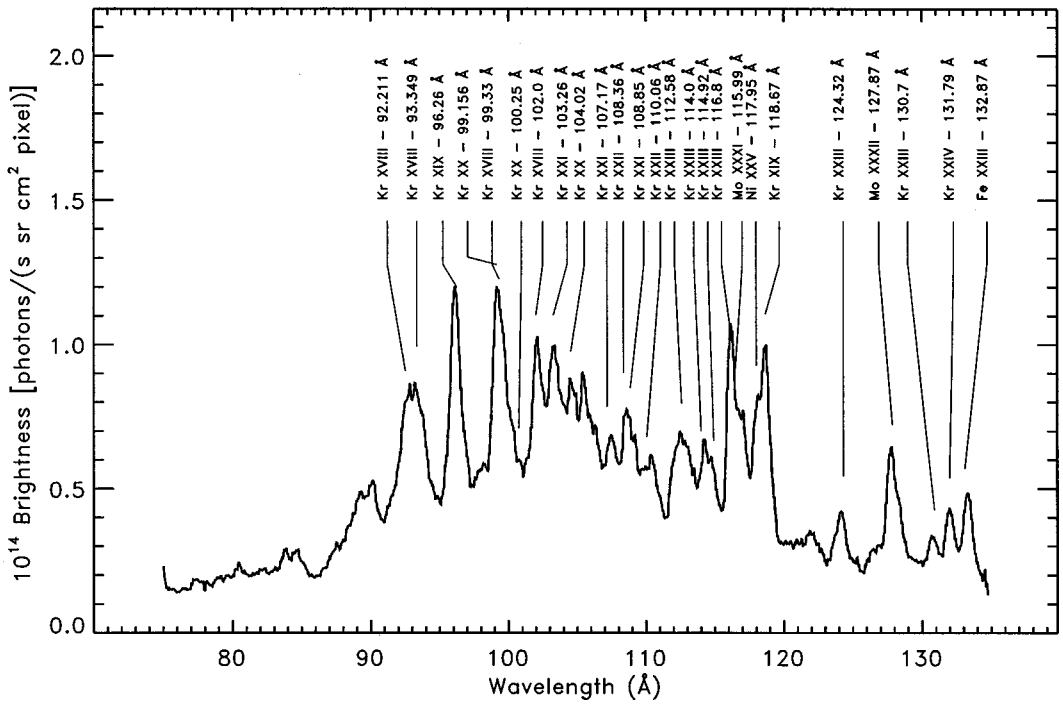

FIG. 4. Kr spectrum from GRITS between 70 and 130 Å.

Argon and krypton were puffed into the tokamak plasma at the beginning of the steady state portion of the plasma ($t = 0.5$ s). The gas was introduced by opening a piezoelectric valve for 2–3 ms. The gas entered the plasma immediately after the puff. The concentration increased until a steady state condition existed in the plasma. For Ar the gas concentration stabilized between 1.3 and 1.5 s. The Kr accumulation in the plasma reached a steady state plateau slightly earlier between 1.2 and 1.4 s. This can be seen in time history of the Ar^{14+} line at 221.15 Å (Fig. 3). The spatial brightness profiles presented for both Ar and Kr are taken during the plateau of the gas puff.

Two photometrically calibrated spectrometers measured the Ar and Kr spectrum and the spatial brightness profiles in the 10 to 1700 Å region. The XUV spectrograph [the grazing incidence time resolving spectrometer (GRITS)] was a 1 m Rowland circle, grazing incidence (at 2°) system with a 1200 groove/mm gold coated grating [17,18]. The detector consisted of a microchannel plate-phosphor-reticon [19]. The wavelength coverage was 10–350 Å with ~60 Å covered by

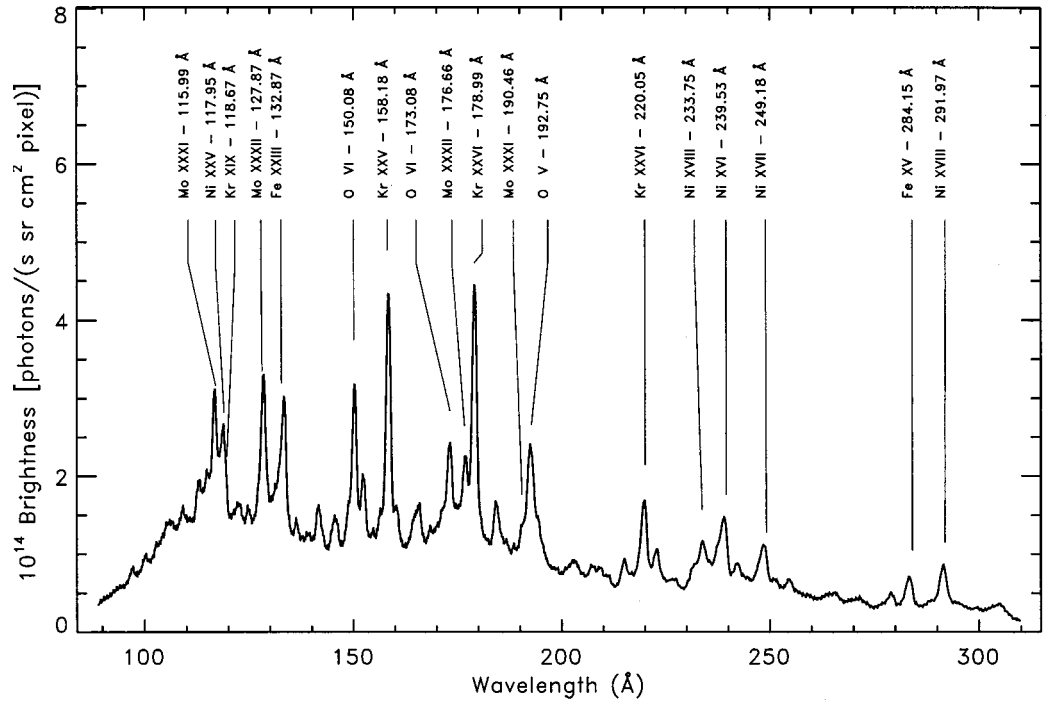

FIG. 5. Kr spectrum from SPRED between 100 and 300 Å.

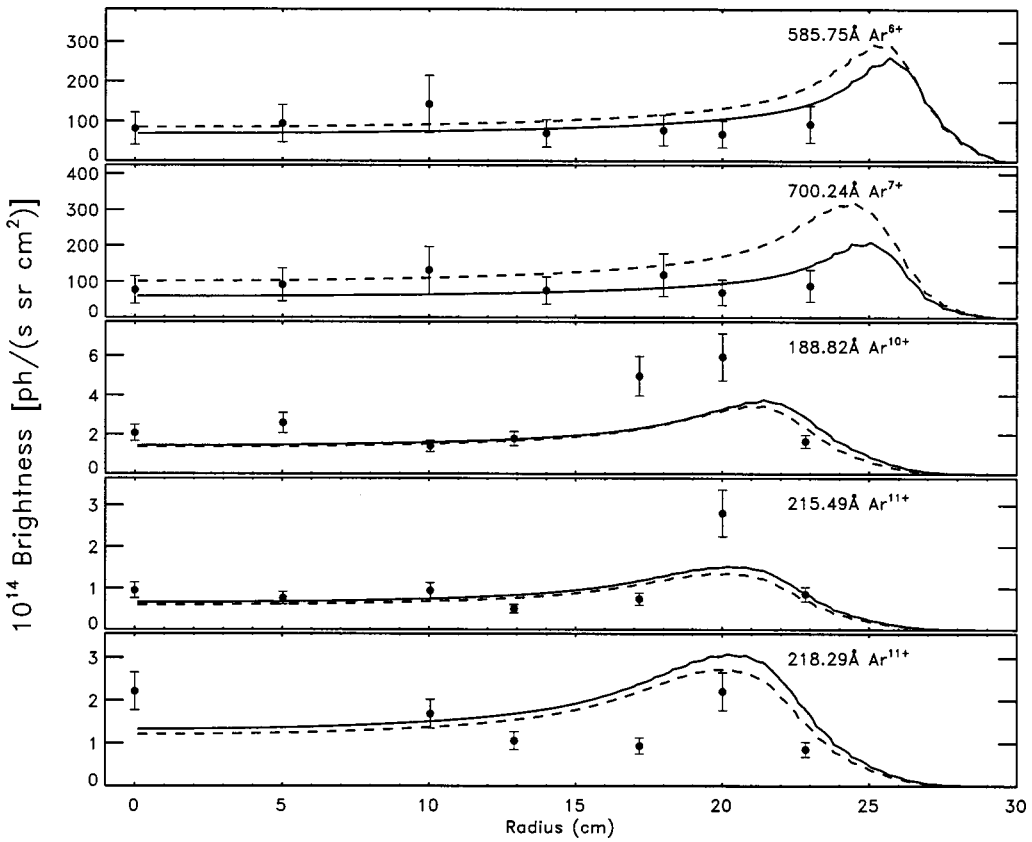

FIG. 6. Experimental and modeled spatial brightness profiles of the Ar^{6+}, Ar^{7+}, Ar^{10+}, and Ar^{11+} lines (FTU). Plotted are the original ionization balance (dashed lines) and the HULLAC/Mazzotta ionization balance (solid lines) which includes DR and EA processes.

the detector during each discharge. This instrument was photometrically calibrated using the SURF II synchrotron facility at the National Bureau of Standards and Technology (NIST) in August 1997. The error on the photometric calibration was $\pm 20\%$.

The vuv spectrometer was a survey, poor resolution, extended domain spectrometer (SPRED) [20]. The longer wavelength grating had 290 groove/mm and covered the 200–1700 Å range in each plasma. The shorter wavelength grating had 2100 groove/mm, and the wavelength coverage was nominally 100–300 Å. The SPRED calibration was directly transferred from the GRITS in the shorter wavelengths and extended to the longer wavelengths by the line ratio technique [21]. The error on the calibration was $\pm 35\%$ at 300 Å and was roughly a factor of 2 at 1000 Å.

Both spectrometers could be positioned on a shot to shot basis to view the plasma from a minor radius of 0 to ~ 25 cm. This spatial range covered the majority of the interesting emission in the plasma. The Kr and Ar spectra at different lines of sight were obtained during a series of similar plasmas. Sample Kr spectra are shown in Figs. 4 and 5 from the GRITS and the SPRED measured along a central line of sight. From these spectra the spatial brightness profiles of the major radiating charge states were obtained. The Ar and Kr emission lines of interest are summarized in Table I.

The measurement of each spatial brightness profile required gas to be puffed into ~ 10 consecutive plasmas. The walls of FTU were cooled to ~ 150 K by liquid nitrogen for impurity control and became loaded with the puffed gas after several plasmas. The residual amount of the puffed gas could be seen on the spectrograph signals (Fig. 3). The background emission from each line was obtained at $t = 0.45$ s, just prior to the gas puff, and was subtracted from that measured during the puff in order to obtain the line brightness for the profiles. The residual gas did not affect the spatial brightness profile measurements. The measured profiles (shown as points) are presented in Figs. 6–8 for Ar^{6+} (Mg-like) to Ar^{17+} (H-like) and Figs. 9 and 10 for Kr^{17+} (K-like) to Kr^{25+} (Na-like) with the simulations from the atomic physics model (lines). The brightness profile of the Kr^{8+} (Ni-like) line was significantly blended with the Mo^{31+} (Na-like) line and could not be used to obtain an accurate profile. The modeling is explained in the following section. The error bars on the experimental points are the uncertainties on the absolute photometric calibration of each line and not the shot to shot uncertainties.

The anomalous impurity particle transport was determined from trace laser blowoff (LBO) injections into the plasma [22] and from visible bremsstrahlung emission [23]. This method was an independent estimation of the particle transport since it did not dependent upon the measurements from the spectrometers. Therefore, the only unknown in the simulations was the ionization/recombination rates. The impurity confinement time, τ_p, can be determined from the exponential time decay of an impurity emission line that was introduced during the LBO injection. This confinement time is related to the particle diffusion, D_p, in the core of the plasma:

$$\tau_p = \left(\frac{a^2}{D_p k^2} \right) \quad \text{for } V_c(r) = 0 \text{ at } r = 0.$$

TABLE I. Kr and Ar lines of interest in FTU tokamak gas puff experiments.

Ionization state	Isoelectronic sequence	Wavelength	Transition
Ar^{6+}	Mg-like	585.75 Å	$2p^6 3s^2$-$2p^6 3s3p(^1S_0-{}^1P_1)$
Ar^{7+}	Na-like	700.24 Å	$2p^6 3s$-$2p^6 3p(^1S_{1/2}-{}^2P_{3/2})$
Ar^{7+}	Na-like	713.812 Å	$2p^6 3s$-$2p^6 3p(^1S_{1/2}-{}^2P_{1/2})$
Ar^{10+}	O-like	188.82 Å	$2s^2 2p4$-$2s2p^5(^3P_2-{}^3P_2)$
Ar^{11+}	N-like	215.49 Å	$2s^2 2p^4$-$2s2p^3(^4S-{}^4P)$
Ar^{11+}	N-like	218.29 Å	$2s^2 2p^4$-$2s2p^3(^4S-{}^4P)$
Ar^{12+}	C-like	210.46 Å	$2s^2 2p^2$-$2s2p^3(^3P-{}^3P)$
Ar^{13+}	B-like	187.95 Å	$2s^2 2p$-$2s2p^2(^2P-{}^2P)$
Ar^{13+}	B-like	194.39 Å	$2s^2 2p$-$2s2p^2(^2P-{}^2S)$
Ar^{14+}	Be-like	221.15 Å	$1s^2 2s^2$-$1s^2 2s2p(^1S_0-{}^1P_1)$
Ar^{15+}	Li-like	353.92 Å	$1s^2 2s$-$1s2p(^1S_{1/2}-{}^2P_{3/2})$
Ar^{15+}	Li-like	389.15 Å	$1s^2 2s$-$1s2p(^1S_{1/2}-{}^2P_{1/2})$
Ar^{16+}	He-like	3.94928 Å	$1s^2$-$1s2p(^1S_1-{}^1P_1)$
Ar^{17+}	H-like	3.737 Å	$1s$-$2p(^2S_{1/2}-{}^2P_{3/2})$
Kr^{8+}	Ni-like	117.7 Å	$3d^{10}$-$3d^9 4p(^1S-{}^3P)$
Kr^{17+}	K-like	92.211 Å	$3p^6 3d$-$3p^5 3d^2(^2D_{3/2}-{}^2D_{3/2})$
Kr^{17+}	K-like	93.349 Å	$3p^6 3d$-$3p^5 3d^2(^2D_{5/2}-{}^2D_{5/2})$
Kr^{17+}	K-like	99.330 Å	$3p^6 3d$-$3p^5 3d^2(^2D_{5/2}-{}^2F_{7/2})$
Kr^{17+}	K-like	102.001	$3p^6 3d$-$3p^5 3d^2(^2D_{3/2}-{}^2F_{5/2})$
Kr^{18+}	Ar-like	96.26 Å	$3p^6$-$3p^5 3d(^1S_0-{}^1P_1)$
Kr^{18+}	Ar-like	118.672 Å	$3p^6$-$3p^5 3d(^1S_0-{}^3D_1)$
Kr^{19+}	Cl-like	99.156 Å	$3p^5 3p^4 3d(^2P_{3/2}-{}^2D_{5/2})$
Kr^{20+}	S-like	103.26 Å	$3p^4$-$3p^3 3d(^3P_2-{}^1F_3)$
Kr^{20+}	S-like	107.17 Å	$3p^4$-$3p^3 3d(^3P_2-{}^2P_2)$
Kr^{21+}	P-like	108.36 Å	$3p^3$-$3p^2 3d(^2D_{5/2}-{}^2F_{7/2})$
Kr^{22+}	Si-like	124.32 Å	$3s^2 3p^2$-$3s^2 3p3d(^3P_1-{}^3P_2)$
Kr^{22+}	Si-like	130.70 Å	$3s^2 3p^2$-$3s^2 3p3d(^1D_2-{}^3D_3)$
Kr^{23+}	Al-like	131.795 Å	$3s^2 3p$-$3s^2 3d(^2P_{3/2}-{}^2D_{5/2})$
Kr^{24+}	Mg-like	158.183 Å	$2p^6 3s^2$-$2p^6 3s3p(^1S_0-{}^1P_1)$
Kr^{25+}	Na-like	178.990 Å	$2p^6 3s$-$2p^6 3p(^1S_{1/2}-{}^2P_{3/2})$
Kr^{25+}	Na-like	220.057 Å	$2p^6 3s$-$2p^6 3p(^1S_{1/2}-{}^2P_{1/2})$

The variables a and k are the minor radius and the first zero of the zeroth-order Bessel function ($\sim$2.405), respectively. $V_c(r)$ is the convective velocity in the plasma. The resonant $2s^2$-$2s2p$ Be-like transitions of Ni (117.9 Å) and Fe (132.7 Å) were used to determine fairly accurately the particle transport in the core plasma. The τ_p from these injections was $\sim$35 ms in ohmically heated FTU tokamak plasmas. Therefore particle diffusion was $\sim$5000 cm^2/s at $r=0$.

The impurity density profile (Fig. 11) was determined from inversions of the free-free bremsstrahlung spatial profiles. The bremsstrahlung is related to the Z_{eff}. This analysis assumed that the change in bremsstrahlung emission during the gas puffs was only produced by the gas. The contribution to the emission from the intrinsic impurities (mostly molybdenum) was subtracted during the analysis. A detailed discussion of this analysis can be found in Ref. [24]. The analysis predicts a reasonably flat impurity density (within experimental error) for radii less than 20 cm. There is no significant spatial distortion of the global impurity gas density due to the anomalous impurity particle transport. This implies little convection and a mostly diffusive plasma. Therefore, a flat diffusion profile of 5000 cm^2/s (for $r<25$ cm) was used in the MIST code and for the brightness profile simulations. This method has greater inherent error and assumptions than the LBO injections and, thus, the transport is less well known in the intermediate zone ($r=15-25$ cm).

B. Alcator C-Mod Tokamak

Alcator C-Mod tokamak operated with very similar parameters to FTU tokamak but had a divertor and a D-shaped plasma cross section. The walls of the tokamak were operated at room temperature and did not saturate with the puffed gas as they did in FTU tokamak plasmas. Ar was puffed into Ohmically heated plasmas with L-mode confinement having a central electron temperature of $\sim$2.7 keV and an central electron density of 1.2×10^{14} particles/cm^3. The anomalous transport on Alcator C-Mod was investigated in detail and found to be mainly diffusive ($D\sim5000$ cm^2/s) in Ohmically heated plasmas with L-mode confinement [25].

The spatial brightness profiles of Ar were measured using a set of five spatially scanning von Hamos type x-ray spectrometers (HIREX) [26]. They used a quartz crystal ($2d=6.687$ Å) and covered the 2.8–4.0 Å spectral range. Kr spectra could not be observed since these emission lines (6–7 Å) were outside of the spectral range of HIREX. Spec-

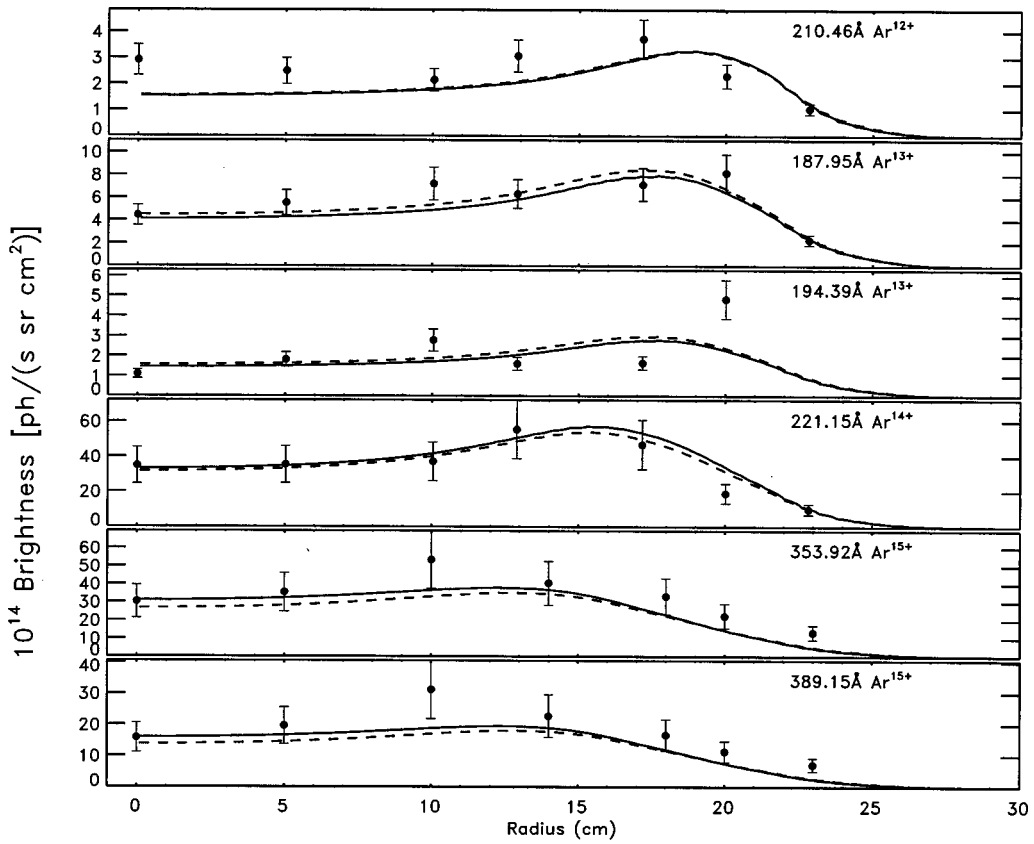

FIG. 7. Experimental and modeled spatial brightness profiles of the Ar^{12+}, Ar^{13+}, Ar^{14+}, and Ar^{15+} lines (FTU). Plotted are the original ionization balance (dashed lines) and the HULLAC/Mazzotta ionization balance (solid lines) which includes DR and EA processes.

tra were collected every 50 ms with 120 mÅ covered during each shot. For this analysis the $1s^2$-$1s2p$ ($^1S_0-{}^1P_1$) He-like line at 3.94928 Å was measured. The HIREX can be spatially scanned to view the entire Alcator C-Mod tokamak plasma on a shot to shot basis. The experiments and MIST simulations on Alcator C-Mod were very similar to those performed at FTU and are not presented here in detail. They are documented elsewhere [27].

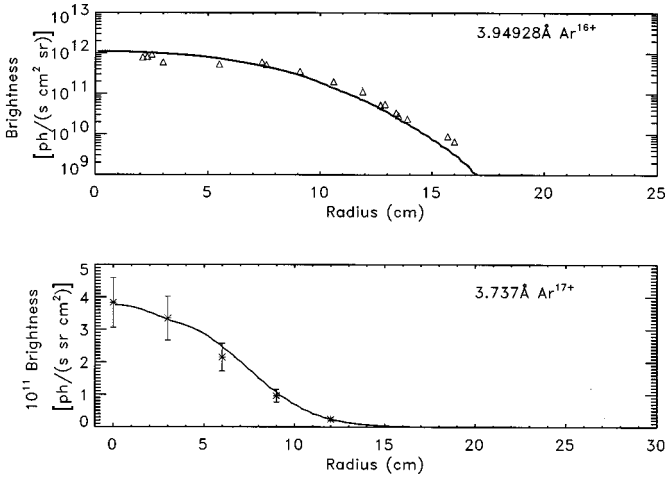

FIG. 8. Experimental and modeled spatial brightness profiles of the Ar^{16+} line (Alcator C-Mod) and Ar^{17+} (FTU). These figures are from two different plasmas. Plotted are the HULLAC/Mazzotta ionization balance (solid lines) which includes DR and EA processes.

III. ATOMIC PHYSICS MODEL AND RATES

The multiple ionization state transport (MIST) [12] code and a collisional radiative model were used to simulate the CSD and the Kr and Ar brightness profiles in the FTU and Alcator C-Mod tokamak plasmas. MIST is a one dimensional (radial in cylindrical coordinates), time dependent impurity transport code which treats the ionization/recombination physics and the trace impurity particle transport simultaneously. Inputs into MIST were the experimentally measured radial electron temperature profile, electron density profile (Fig. 2) and the puffed gas concentration. MIST was run in the time independent mode and determined the impurity CSD of the ionized gas in the plasma with a given set of ionization/recombination rates.

The rates were either the original rates or the rates specifically chosen/calculated for these experiments. The original electron ionization rates in MIST included direct impact (DI) ionization computed using the formula of Lotz [28]. The MIST code did not include excitation-autoionization (EA) rates for either krypton or argon. The original recombination processes included both radiative recombination (RR) and dielectronic recombination (DR), the latter being approximated by the formulas of Burgess and Mertz [29,30,31]

From the previous experiments by Rice *et al.* for molybdenum [14] in Alcator C-Mod tokamak plasmas the DI and RR rates in MIST were found to be accurate for predicting the CSD for Mo, but EA rates had to be added and the DR rates needed to be changed. Therefore, the DI and RR rates for Kr

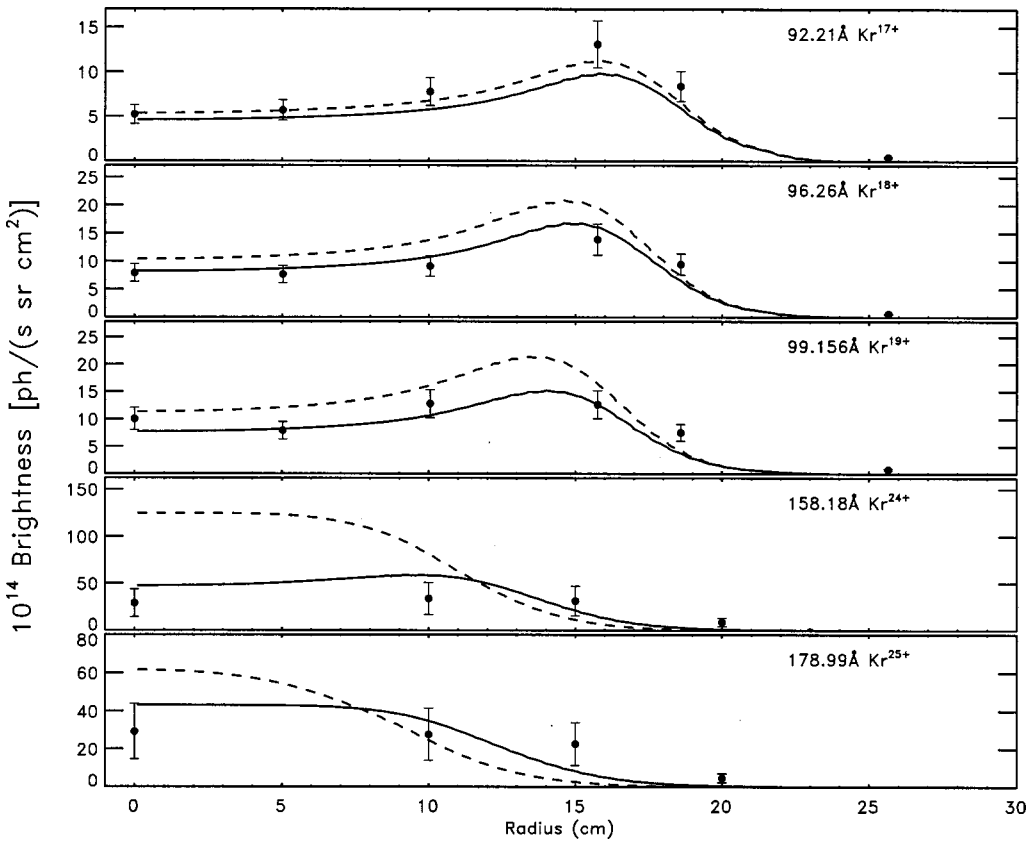

FIG. 9. Experimental and modeled spatial brightness profiles of the Kr^{17+}, Kr^{18+}, Kr^{19+}, Kr^{24+}, and Kr^{25+} emission lines (FTU). Plotted are the original ionization balance (dashed lines) and new ionization balance (solid lines) which includes DR and EA processes.

and Ar in MIST were used for all the present simulations. To obtain accurate excitation-autoionization and dielectronic recombination rates for krypton and argon [32], *ab initio* calculations were performed by using the atomic physics package HULLAC or were taken from the compilation of Mazzotta. The excitation-autoionization rates for Kr^{20+}-Kr^{25+} and Ar^{1+}-Ar^{16+} were provided by HULLAC. The DR rates for Ar^{1+}-Ar^{17+} were those given by Mazzotta. Excitation-autoionization rates calculated by Mitnik with HULLAC [33] were also included for the Kr^{7+} (Cu-like) -Kr^{0+} (Kr-like) ions.

A collisional radiative (CR) model determined the intensities from each Ar and Kr line of interest. Collisional excitation rates and photodecay rates provided by HULLAC and the CSD provided by the MIST codes were incorporated into the sophisticated collisional radiative model (COLRAD) in HULLAC for the lines listed in Table I. The emissivity of each line was calculated for each radial magnetic flux surface of the circular plasma for FTU and the D-shaped plasma of the Alcator C-Mod tokamak. The flux surfaces used in the MIST were on a grid of 50 points between $r/a=0$ to 1.1 separated equally in radius. These emissivities were summed over the line of sight of the spectrometers to produce a synthetic brightness of each spectral line. The synthetic brightness profiles were constructed by computing the line brightness for each line of sight of the spectrometers (Figs. 6–10). Two sets of synthetic brightness profiles were generated. The first based on the CSD computed with the original ionization/recombination rates in MIST and the second based on the CSD computed with the rates from HULLAC and Mazzotta as detailed above.

The total radative losses from each impurity were calculated from the CR model at each temperature. The radiation loss channels are dominated by spectral line emission. The transitions of several thousand lines including transitions between excited states were included. Also included were the radiation channels of bremsstrahlung, radiative recombination and dielectronic recombination. Summing all the radiation channels produced a radiative cooling rate curve. One must understand that the CR model utilized the CSD determined from the rates generated by HULLAC. The CSD was confirmed by the experimental spatial brightness profiles. Therefore, the atomic physics rates in the cooling curves were significantly constrained by experiment. The direct comparisons between the bolometric spatial profiles and the radiative cooling curves confirm the validity of the HULLAC calculations.

IV. SPATIAL PROFILES

For Ar the spatial brightness profile simulations with the original rates and with the more accurate HULLAC and Mazzotta rates are compared with the experimentally measured points for Ar^{6+}, Ar^{7+}, Ar^{10+}, and Ar^{11+} in Fig. 6 (FTU), for Ar^{12+}, Ar^{13+}, Ar^{14+}, and Ar^{15+} in Fig. 7 (FTU) and for Ar^{16+} (C-Mod) and Ar^{17+} (FTU) in Fig. 8. The simulated brightness profiles using the more accurate (solid lines: HULLAC and Mazzotta) atomic rates predicted the measured radial brightness profiles slightly better than the

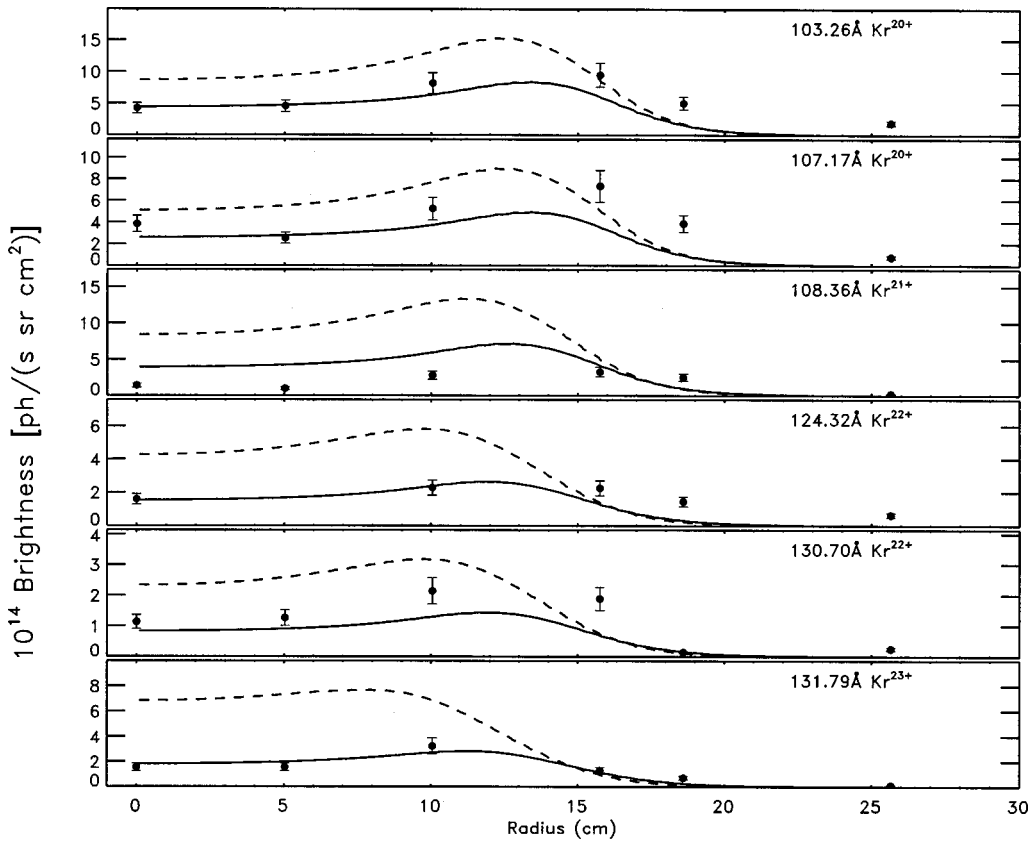

FIG. 10. Experimental and modeled spatial brightness profile of the Kr^{20+}, Kr^{21+}, Kr^{22+}, and Kr^{23+} emission lines (FTU). Plotted are the original ionization balance (dashed lines) and new ionization balance (solid lines) which includes DR and EA processes.

simulations using the older physics rates (dashed lines). The weaker emission from Ar^{10+}, Ar^{11+}, and Ar^{13+} lines made the comparison more difficult. The x-ray line measured in the Alcator C-Mod tokamak also showed good agreement between the experiment and the simulations. The differences between the two models of the He like lines were trivial. Only the HULLAC/Mazzotta model is show in Fig. 8. The more accurate HULLAC/Mazzotta atomic physics rates for Ar did not significantly alter the CSD or the simulated spatial brightness profiles since Ar is a reasonably understood low Z element and fairly straightforward to model. The derived Ar impurity density was $\sim 0.003\ n_{e0}$ (1.9×10^{11} particles/cm^3) in FTU. The Ar density in Alcator C-Mod tokamak was $\sim 0.002\ n_{e0}$ (2.9×10^{11} particles/cm^3).

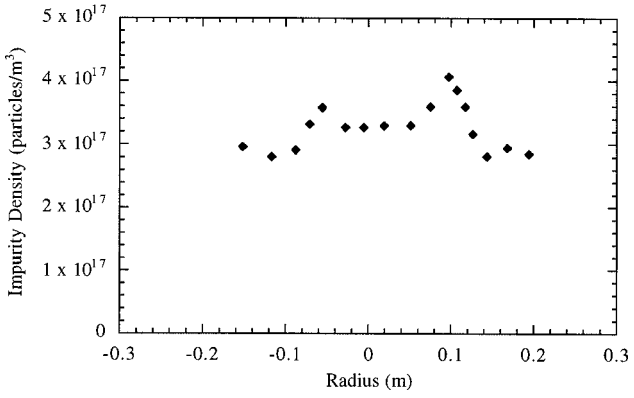

FIG. 11. Argon impurity density profile derived from visible bremsstrahlung.

The effect of the different atomic physics rates upon the simulations for Kr were much more significant than for those of argon. This can be seen in Fig. 9 for Kr^{17+}, Kr^{18+}, Kr^{19+}, Kr^{24+}, and Kr^{25+} and Fig. 10 for Kr^{20+}, Kr^{21+}, Kr^{22+}, and Kr^{23+}. The simulations with the original atomic physics rates in MIST were inadequate to predict the experiment. The simulations which included the HULLAC rates more accurately predicted the measured brightness profiles although some discrepancies do exist. One must note that only a selected set of the HULLAC rates were included. The HULLAC rates provide a significant improvement over the existing rates. This improvement is especially true for the Kr^{24+} and Kr^{25+} ionization states. The old rates would predict a significant ($\sim 2\times$) enhancement in the abundances of these charge states with respect to the abundances of Kr^{17+} and Kr^{18+}. Using the resonant lines of Kr^{24+} and Kr^{25+}, the Kr density in the plasma was predicted to be $\sim 0.0006\ n_{e0}$ (4.6×10^{10} particles/cm^3) with the HULLAC CSD and $\sim 0.0012\ n_{e0}$ (9.2×10^{10} particles/cm^3) with the original CSD. With the simultaneous measurement of the majority of the charge states in the plasma, the CSD of Kr (and Ar) can be considered to be well constrained. No serious discrepancies existed between the HULLAC simulation and the experiment. The CSD created with the original rates in MIST is shown with the CSD created with the HULLAC rates in Fig. 12.

The major correction to the ionization/recombination rates in the MIST was the inclusion of the EA rates. The same conclusion was reached by Rice *et al.* for molybdenum [14]. Therefore, the EA rates for high-Z impurities must be in-

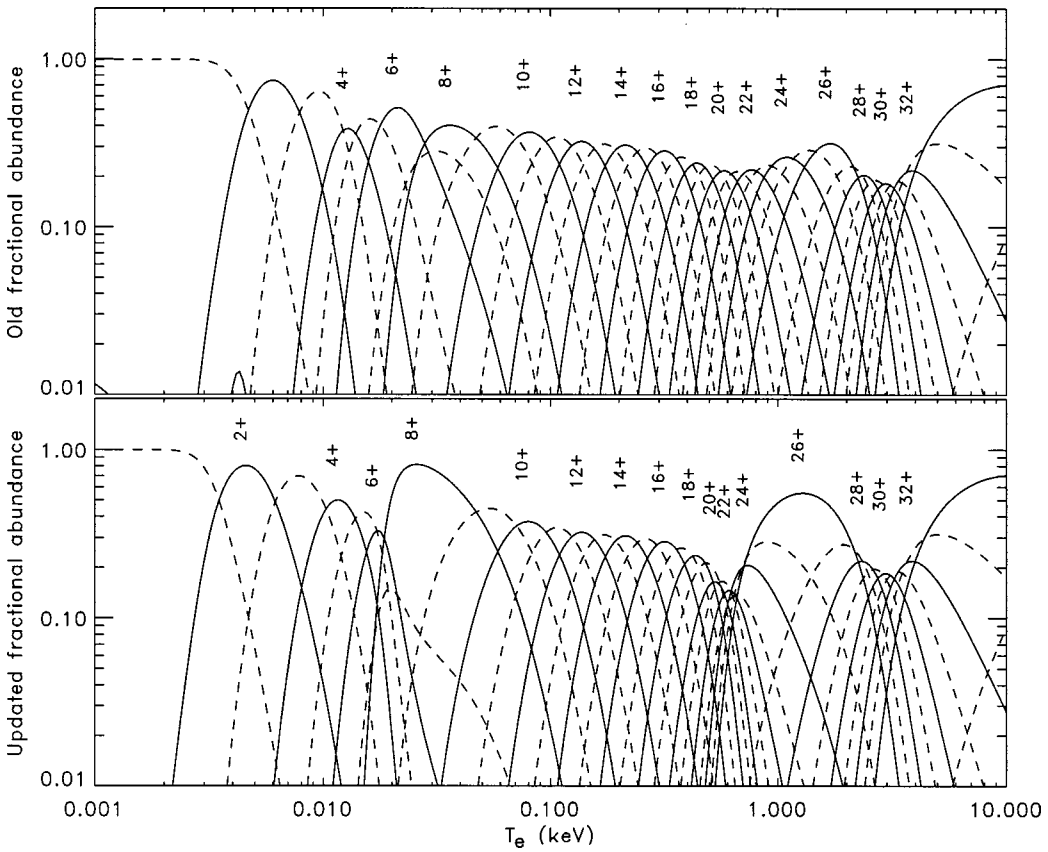

FIG. 12. CSD of Kr with the original rate in the MIST and the up to data rates in the MIST.

cluded when calculating the CSD in a tokamak plasma. Without these rates the CSD will not be correct. If the EA rates were not included, agreement between the simulation and the experiment could only be obtained by adjusting the anomalous transport. This would alter the relative abundance of the charge states. The resulting impurity density would be assumed to be (incorrectly) hollow with an outward flux. The radiative cooling predictions would also be incorrect.

V. COOLING RATE CURVES

Cooling curves for both Kr and Ar were computed using the HULLAC code and the ADPAK atomic data package. The predicted radiation from these two curves was compared with the emissivity profiles measured by the bolometery. The Ar cooling curve has been discussed thoroughly in Ref. [30]. Therefore, only the results for Kr are presented here. The emissivity profiles of a sample ohmically heated FTU tokamak plasma into which Kr was puffed is presented in Fig. 13. The input power was ~1000 kW from the Ohmic heating coils. The krypton density was $\sim 4.7 \times 10^{10}$ particles/cm^3 as determined from the spectrometers and the MIST transport code. The T_{e0} was 1.1 keV, and the n_{e0} was 1.84×10^{14} particles/cm^3. Spectroscopy indicated that as the radiation from krypton increased during the gas puff, the radiation from the intrinsic impurities significantly decreased (by ~ factor of 10). Therefore, most of the impurity radiation that was measured by the bolometers was emitted from Kr ions. The emissivities were simulated with four radiative cooling curves: three from HULLAC [34] and one from ADPAK by Post. Two of the HULLAC cooling curves were at ionization equilibrium (no transport) and included different CSD's: one was the older CSD originally in MIST and other was created by using the HULLAC rates. The third HULLAC cooling curve included the HULLAC CSD with a diffusion of 5000 cm^2/s. To produce emissivities from these cooling curves, one needs the impurity density profile from the MIST transport code and the measured electron density

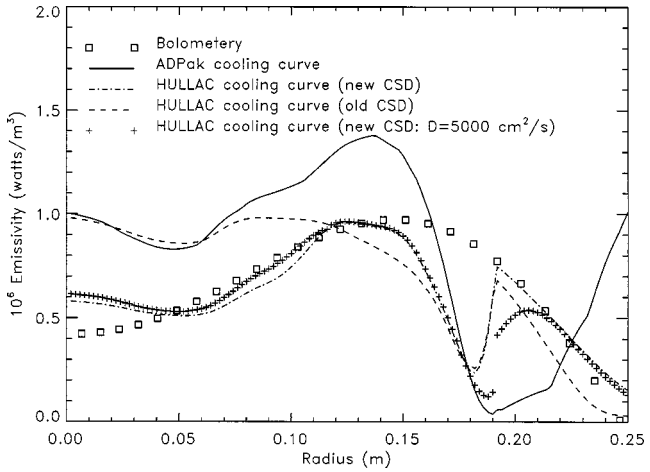

FIG. 13. Comparison of the measured emissivity profile from krypton from bolometery with the calculated emissivity profiles from the HULLAC and the ADPAK cooling curves. Three HULLAC curves, one with the old CSD at ionization equilibrium, one with the new CSD at ionization equilibrium, and one with the new CSD and a $D = 5000$ cm^2/s (with EA and DR rates), show the shift in the cooling to lower temperatures with the correct CSD.

and electron temperature profiles.

The Kr emissivity from the HULLAC cooling curve with the HULLAC CSD was in good agreement with the bolometery profile. The HULLAC cooling curve with the older CSD yielded a much poorer agreement with the bolometery. With the older CSD the predicted radiation from the core ($r/a < 0.5$) of the plasma was too large. This confirms the need for a correct CSD in the cooling curve calculations. The HULLAC CSD had a significant effect on the cooling curve and shifted the bulk of the radiation to lower temperatures since the maximum abundance of the radiators now occurs at lower temperatures [35].

The major discrepancy between the bolometery and the HULLAC cooling curve simulations occurs at ~16 cm. The simulated radiation under predicts the radiation here and leaves a small gap. There are three possible explanations for this: particle transport, significant radiation from another impurity or a problem with the bolometric measurements. Particle transport can shift or spread the CSD in radius. This could blur and fill in the gaps in the predicted emissivity profile. However, including the transport in the calculations does not account for the small gap as can be seen in Fig. 13. Furthermore, the simulated profile with no transport does not significantly differ from the profile that included a diffusion of 5000 cm^2/s in the CSD. This is similar to the conclusion in a previous work in which the anomalous particle transport was not found to effect significantly the emissivities predicted by the HULLAC cooling curve [36]. The major low-Z impurity present in FTU is oxygen. Simulations using the ADPAK oxygen cooling curve do not account for the missing radiation., The oxygen radiation peaks near the edge (20–25 cm). The most likely explanation for the discrepancy is a problem with the bolometric data. The bolometer has a spatial resolution of ~2 cm. This is too coarse to resolve fine details within the spatial extent of the discrepancy which is ~ 3 cm. Also, the bolometric emissivities are produced from an inversion of line integrated measurements using Zernicke polynomials. The process used Zernicke polynomials of low order ($K=3$) and could not yield the detailed radial fine structure predicted by the simulations.

The cooling curve calculated by ADPAK did not correctly predict the measured emissivities. This cooling rate curve did not explicitly include any ionization balance calculations, but instead assumed the presence of a single fictitious ''average ion,'' although ionization/recombination rates (the original ones in the MIST) were used to calculated the average ion. This average ion model assumed a single Z at a give temperature which is not very physical. This method also did not use a collisional radiative model. Instead, transitions between average levels were used to calculate the line radiation. Estimates for the bremsstrahlung, and recombination processes were included. For this plasma, the emissivity profile calculated with the ADPAK model cooling curve significantly overestimated the radiated power from krypton. The predicted emissivity from the core ($r/a<0.3$) was very similar to that predicted by the HULLAC cooling curve with the original CSD in MIST. This implies a problem with the ionization/recombination rates. Much more power was radiated from the middle section of the plasma ($0.6>r/a>0.3$) than was observed. In the outer third of the plasma, the ADPAK model was completely inadequate to describe the radiation patterns. Therefore, this model could not be used to predict correctly the radiated power from krypton.

VI. CONCLUSION

Kr and Ar have been puffed into FTU and Alcator C-Mod tokamak plasmas. Both the L and M-shell spectrum have been measured by photometrically calibrated spectrometers in the 3–1700 Å region. The spatial brightness profiles of this emission and bolometery emissivities have been obtained in a set of similar plasmas to validate ionization/recombination/excitation atomic physics rates used to determine the CSD and the cooling rate curve in a tokamak plasma. The atomic physics rates chosen for this work include EA, DR, collisional excitation and radiative decay rates computed *ab initio* by the HULLAC atomic code and from the compilation of Mazzotta. These rates were input into the MIST impurity transport code to simulate the spatial brightness profiles. These profiles with the more accurate physics rates are in good agreement with the experiment. The predictions using the original rates in the MIST were adequate to simulate Ar but inadequate for Kr. The inclusion of the EA in the MIST produced the most significant improvement in the simulations. These atomic physics rates and CSD are significantly constrained since the majority of the Kr and Ar charge states are measured. The emissivities derived from the cooling rate curves from ADPAK and HULLAC were compared with those from bolometery. The HULLAC curves simulate the emissivities fairly well. The simulations from the ADPAK cooling curves were not satisfactory and over estimated the radiation.

ACKNOWLEDGMENTS

The authors would like to thank the entire FTU and Alcator C-Mod staff for the expert operation of their respective tokamaks and for the use of their facilities. We also thank the Princeton Plasma Physics Laboratory for use of the MIST transport code. This work was supported by U.S. DOE Grant No. DE-FG02-86ER53214 at JHU, Contract No. W-7405-ENG-48 at LLNL, and Contract No. DE-FC02-99ER54512 at MIT.

[1] J. N. Brooks, D. N. Ruzic, D. B. Hayden, and R. B. Turkot, Jr., J. Nucl. Mater. **222**, 143 (1995).
[2] D. M. Meade, Nucl. Fusion **14**, 289 (1974).
[3] T. Tanabe, N. Noda, and H. Nakamura, J. Nucl. Mater. **196-198**, 11 (1992).
[4] G. McCracken, Nucl. Fusion **19**, 923 (1979).
[5] W. P. West, S. L. Allen, N. H. Brooks, D. A. Buchenauer, T. N. Carlstrom, J. W. Cuthbertson, E. J. Doyle, T. E. Evans, M. E. Fentermacher, D. N. Hill, A. W. Hyatt, R. C. Isler, G. L. Jackson, R. Jong, C. C. Klepper, C. J. Lasnier, A. W. Leonard, M. A. Mahdavi, R. Maingi, G. R. McKee, W. H. Meyer, R. A. Moyer, D. G. Nilson, T. W. Petrie, G. D. Porter, T. L. Rhodes, M. J. Schaffer, R. D. Stambaugh, D. M. Thomas, S. Tugarinov, M. R. Wade, J. G. Watkins, D. G. Whyte, and R.

D. Wood, Plasma Phys. Controlled Fusion **39**, A295 (1997).
[6] J. A. Goetz, C. Kurz, B. LaBombard, B. Lipschultz, A. Niemczewski, G. M. McCracken, J. L. Terry, R. L. Boivin, F. Bombarda, P. Bonoli, C. Fiore, S. Golovato, R. Granetz, M. Greenwald, S. Horne, A. Hubbard, I. Hutchinson, J. Irby, E. Marmar, M. Porkolab, J. Rice, J. Snipes, Y. Takase, R. Watterson, B. Welch, S. Wolfe, C. Christensen, D. Garnier, D. Jablonski, D. Lo, D. Lumma, M. May, A. Mazurenko, R. Nachtrieb, P. O'Shea, J. Reardon, J. Rost, J. Schachter, J. Sorci, P. Stek, M. Umansky, and Y. Wang, Phys. Plasmas **3**, 1908 (1996).
[7] J. Rapp, G. Van Oost, G. Bertschinger, L. Konen, H. R. Koslowski, A. Kramer-Flecken, A. Messiaen, J. Ongena, V. Phillips, A. Pospieszczyk, U. Samm, T. Tanabe, G. Telesca, M. Z. Tokar, and B. Unterberg, in *Proceedings of the 24th European Physical Society Conference on Controlled Fusion and Plasma Physics* (European Physical Society, Florence, 1997), Vol. 21A, Pt. IV, p. 1745.
[8] G. F. Matthews for the JET Team, JET Report No. JET-P(95) 40 (1995).
[9] A. Bar-Shalom, M. Klapisch, and J. Oreg, Phys. Rev. A **38**, 1773 (1988).
[10] M. Klapisch, Comput. Phys. Commun. **2**, 269 (1971).
[11] M. Klapisch, J. Opt. Soc. Am. **67**, 148 (1977).
[12] R. A. Hulse, Nucl. Technol./Fusion **3**, 259 (1983).
[13] P. Mazzotta, G. Mazzitelli, S. Colafrancesco, and N. Vittorio, Astron. Astrophys., Suppl. Ser. **133**, 403 (1998).
[14] J. E. Rice, J. L. Terry, K. B. Fournier, M. A. Graf, M. Finkenthal, M. J. May, E. S. Marmar, W. H. Goldstein, and A. E. Hubbard, J. Phys. B **29**, 2191 (1995).
[15] D. E. Post, R. V. Jensen, C. B. Tarter, W. H. Grasberger, and W. A. Lokke, At. Data Nucl. Data Tables **20**, 397 (1977).
[16] M. Grolli, in *Proceedings of the International School of Plasma Physics ''Piero Caldirola'' Diagnostics for Contemporary Fusion, Varenna, Italy, 1991*, edited by P. E. Stott, D. K. Akulina, G. Gorini, and E. Sindoni (Editrice Compositori, Bologna, Italy, 1991), pp. 721–729.
[17] B. C. Stratton, H. W. Moos, W. L. Hodge, S. Suckewer, J. C. Hosea, R. A. Hulse, D. Q. Hwang, and J. R. Wilson, Nucl. Fusion **24**, 767 (1984).
[18] W. L. Hodge, B. C. Stratton, and H. W. Moos, Rev. Sci. Instrum. **55**, 1 (1984).
[19] Trademark of EG&G.
[20] R. J. Fonck, Appl. Opt. **21**, 2115 (1982).
[21] M. A. Graf, doctoral thesis, Department of Nuclear Engineering, Massachusetts Institute of Technology, 1995.
[22] F. H. Seguin, R. Petrasso, and E. S. Marmar, Phys. Rev. Lett. **51**, 455 (1983).
[23] D. Pacella, B. C. Gregory, M. Leigheb, G. Pizzicaroli, G. Mazzitelli, M. Borra, L. Pieroni, M. May, K. B. Fournier, W. H. Goldstein, M. Finkenthal, M. Mattioli, F. Alladio, B. Angelini, M. L. Apicella, G. Apruzzese, E. Barbato, S. Belforte, L. Bertalot, A. Bertocchi, G. Bracco, A. Bruschi 5, G. Buceti, P. Buratti, A. Cardinali, C. Castaldo, C. Centioli, R. Cesario, P. Chuilon, S. C. Cianfarani, S. Ciattaglia, S. Cirant, V. Cocilovo, F. Crisanti, R. De Angelis, F. De Marco, B. Esposito, D. Frigione, L. Gabellieri, G. Gatti, E. Giovannozzi, C. Gourlan, F. Gravanti, G. Gravanti, G. Granucci 5, M. Grolli, F. Iannone, H. Kroegler, G. Maddaluno, G. Maffia, M. Marinucci, P. Micozzi, F. Mirizzi, F. P. Orsitto, L. Panaccione, M. Panella, V. Pericoli-Ridolfini, S. Podda, G. B. Righetti, F. Romanelli, F. Santini, M. Sassi, S. E. Segre, E. Stemini, A. Simonetto, C. Sozzi, N. Tartoni, B. Tilia, A. A. Tuccillo, O. Tudisco, V. Vitale, G. Vlad, V. Zanza, M. Zerbini, and F. Zonca, in *Proceedings of the 25th European Physical Society Conference on Controlled Fusion and Plasma Physics, Prague, 1998* (European Physical Society, Florence, 1998), Vol. 22C, pp. 862–865.
[24] D. Pacella, B. C. Gregory, L. Gabellieri, G. Mazzitelli, M. Leigheb, G. Pizzicaroli, K. B. Fournier, W. H. Goldstein, M. May, and M. Finkenthal, in *Proceedings of the 25th European Physical Society Conference on Controlled Fusion and Plasma Physics, Prague, 1998* (Ref. [23]), Vol. 22C.
[25] J. E. Rice, J. L. Terry, J. A. Goetz, Y. Wang, E. S. Marmar, M. Greenwald, I. Hutchinson, Y. Takase, S. Wolfe, H. Ohkawa, and A. Hubbard, Phys. Plasmas **4**, 1605 (1997).
[26] J. E. Rice and E. S. Marmar, Rev. Sci. Instrum. **61**, 2753 (1990).
[27] M. J. May, M. Finkenthal, S. P. Regan, H. W. Moos, J. L. Terry, J. A. Goetz, M. A. Graf, J. E. Rice, E. S. Marmar, K. B. Fournier, and W. H. Goldstein, Nucl. Fusion **37**, 881 (1997).
[28] W. Lotz, Astrophys. J., Suppl. **14**, 207 (1967).
[29] A. Burgess, Astrophys. J. **139**, 766 (1964).
[30] A. Burgess, Astrophys. J. **141**, 1588 (1965).
[31] A. Mertz, R. Cowan, and N. Magee, Los Alamos Scientific Laboratory Report No. LA-6220-MS (1976).
[32] K. B. Fournier, M. Cohen, M. J. May, and W. H. Goldstein, At. Data Nucl. Data Tables **70**, 231 (1998).
[33] D. Mitnik, P. Mandelbaum, J. L. Schwob, A. Bar-Shalom, J. Oreg, and W. H. Goldstein, Phys. Rev. A **50**, 4911 (1994).
[34] K. B. Fournier, M. J. May, D. Pacella, B. C. Gregory, J. E. Rice, J. L. Terry, M. Finkenthal, and W. H. Goldstein, in *Proceedings of the 11th Conference on Atomic Process in Plasmas, Auburn, AL*, AIP Conf. Proc. No. 443 (AIP, Woodbury, NY, 1998), pp. 73–83.
[35] K. B. Fournier, D. Pacella, M. J. May, M. Finkenthal, and W. H. Goldstein, Nucl. Fusion **37**, 825 (1997).
[36] M. J. May, K. B. Fournier, J. A. Goetz, J. L. Terry, D. Pacella, M. Finkenthal, E. S. Marmar, and W. H. Goldstein, Plasma Phys. Controlled Fusion **41**, 45 (1999).